REMOTE TRIGGERING OF MICROSEISMICITY IN ANTARCTICA BY LARGE DISTANT EARTHQUAKES

A Dissertation
Presented to
The Academic Faculty

by

Mingyu Ji

In Partial Fulfillment
of the Requirements for the Degree
Master of Science in the
School of Earth and Atmospheric Sciences

Georgia Institute of Technology
August 2019

REMOTE TRIGGERING OF MICROSEISMICITY IN ANTARCTICA BY LARGE DISTANT EARTHQUAKES

Approved by:

Dr. Zhigang Peng, Advisor
School of Earth and Atmospheric Sciences
Georgia Institute of Technology

Dr. Andrew V. Newman
School of Earth and Atmospheric Sciences
Georgia Institute of Technology

Dr. Sven Simon
School of Earth and Atmospheric Sciences
Georgia Institute of Technology

Date Approved: July 25, 2019

ACKNOWLEDGEMENTS

I would like to thank my advisor Dr. Zhigang Peng a lot for his guidance on both my academic study and personal life, and his patience and kindness. I thank my thesis committee members, Dr. Andrew Newman and Dr. Sven Simon for reviewing my thesis and providing many critical suggestions and comments. I would also like to thank GT's geophysical faculty, including Dr. Joe Dufek, Dr. Ken Ferrier, Dr. Felix Herrmann for the instruction on both course works and research. My special gratitude to Dr. Taillefert Martial and Olivia Kulisz for the warm help offered without doubt. I thank many graduate students and my friends for the encouragement and help, including Chenyu Li, Dongdong Yao, Qiushi Zhai, Miguel Neves, Weilai Pei, Zax Zhang and the rest of crew. Thanks to my family for supporting me through many years. Finally, a sincere thank to Qiyang Yan for being there with me during my difficult time. Too many to list here. Luckily, you all will probably never read this, but I will make sure to tell you all about it...

TABLE OF CONTENTS

LIST OF TABLES

LIST OF FIGURES

SUMMARY

Recent studies suggested that seismic waves from significant earthquakes could trigger shallow seismic events and deep tremor in tectonically active regions at the long-distance range. Dynamic stresses carried by teleseismic waves can promote failure on the critically stressed faults at depth and trigger local microseismicity. This phenomenon is also known as remote triggering. However, only a few remote triggering studies have been done in Antarctica, mostly due to sparse network coverage. Since 2007, a new generation of broadband sensors has been deployed as permanent stations throughout Antarctica (POLENET project). This, together with other permanent and temporary seismic stations, provides critical infrastructure to investigate the remote triggering effect in Antarctica. In this study, we examine remotely triggered seismicity following large distant mainshocks since 2000 with visual inspection on raw waveforms and spectrograms. We identify evidence of possible triggered local events at various stations during or immediately following the surface waves of the 2010 Mw8.8 Maule, 2012 Mw8.6 Indian Ocean and 2016 Mw7.8 Kaikoura earthquakes. We also focus on how large distant earthquakes since 2000 triggered seismic activity around Mt. Erebus using broadband station IU.SBA, and find an apparent triggering threshold of 4-6KPa. Besides, we examine the spatial distribution of remote triggering with tectonic background and ice movement of Antarctica. Our results are consistent with previous inferences that most triggered events occur within West Antarctica and Antarctic Peninsula with rapid glacier movement and tectonic activity as compared to stable East Antarctica.

CHAPTER 1. INTRODUCTION

1.1 Overview

Improved observational condition and evidence in the last twenty years suggest that seismic waves from large distant earthquakes are capable of dynamically triggering and modulating local seismic or aseismic activity at thousands of kilometers distance [Hill and Prejean, 2015; Peng and Gomberg, 2010]. These remotely triggering effects/activities occur mostly during or shortly after the passage of surface waves and in tectonically active regions, such as geothermal/volcanic systems or plate boundary faults. Surface waves from teleseismic events instantaneously raise the local dynamic stress at depth and promote slip on the faults that are critically stressed and close to failure [Hill, 2012].

In recent years, a new generation of geodetic and seismic instrumentation has been deployed as permanent stations throughout Antarctica (POLENET), in addition to the existing permanent and temporary stations, which provide critical infrastructure needed to answer fundamental questions about both crustal-scale tectonic structures and ice sheets, and their interactions. Concurrent with this increase in Antarctic stations is a recent global increase in the number of large earthquakes (> Mw7.5), especially after the 2004 Mw9.1 Sumatra earthquake [Lay, 2015]. In this study, we search for evidence of the remote triggering effect on Antarctica and neighboring regions following recent large earthquakes globally, including the 2004 Mw9.1 Sumatra, 2010 Mw8.8 Maule, 2011 Mw9.1 Tohoku, 2012 Mw8.6 Indian Ocean, 2014 Mw8.2 Chile, 2015 Mw8.3 Chile and 2016 Mw7.8 Kaikoura earthquakes (**Figure 1**). We also examine the triggering threshold near Mt. Erebus, a heavily glaciated large stratovolcano on the Ross Island, as well as the spatial

distribution of remote triggering sites and its relationship with tectonic background and glacial movements in Antarctica.

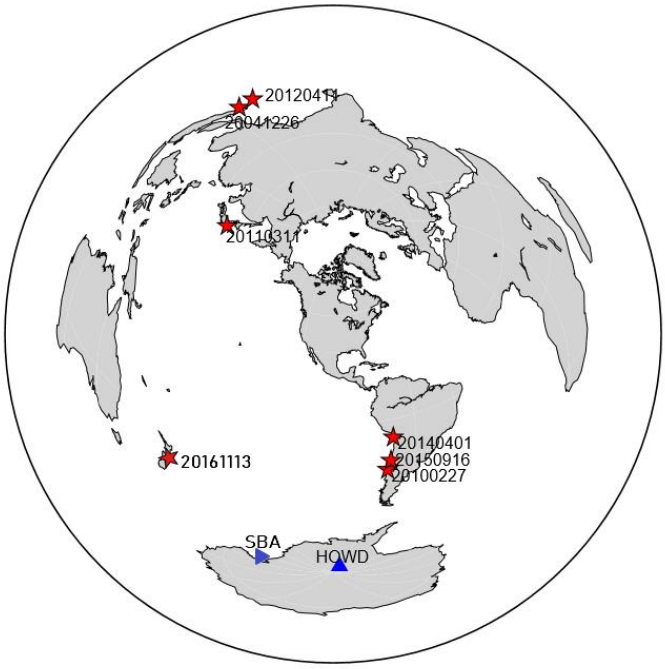

Figure 1. Global distribution map of selected events (red stars), including the 2004 Sumatra, 2010 Maule, 2011 Tohoku, 2014 Indian Ocean, 2014 & 2015 Chile and 2016 Kaikoura earthquakes as mentioned in Chapter 1, and two stations (blue triangles) with clear remote triggering effects, IU.SBA and YT.HOWD. The latter YT.HOWD is marked as clear triggering phenomenon by previous studies [Peng et al., 2014].

Improved knowledge of how the Antarctic ice sheet responds to external perturbations such as dynamic stresses from large distant earthquakes and recent ice unloading could lead to a better understanding of ice failure and related dynamic processes. It can also lead to a better classification between icequake, tectonic earthquakes and volcanic activities in Antarctica. In particular, we seek to comprehensively analyze triggered events at various stations, identify possible triggering thresholds of dynamic stress change for triggering mircroseismicity by teleseismic waves. We also try to build an updated triggering sensitivity map throughout the continent, and compare with the tectonic background and ice sheet movement in Antarctica. Both possible triggering stress threshold and triggered map would contribute to a better understanding of stress levels in the crust and volcanic/glacier environments, potential physical mechanisms of remote triggering effect and influence on glacier dynamics.

1.2 Previous Studies

Earth's cryosphere is a major component of the solid Earth system, and is similar to shallow crust in many ways. Hence, standard seismological methods and techniques used for studying crustal structures and earthquakes are feasible through the study on various dynamic processes in Antarctica [Aster and Winberry, 2017]. However, cryospheric systems are more complex and nonlinear compared to the regular crust. Thus, seismic sources can be identified and differentiated into three types by interaction objects, which are sources associated with ice-ice dynamic processes, with ice-rock stick-slip and with ice-water interactions (**Figure 2**).

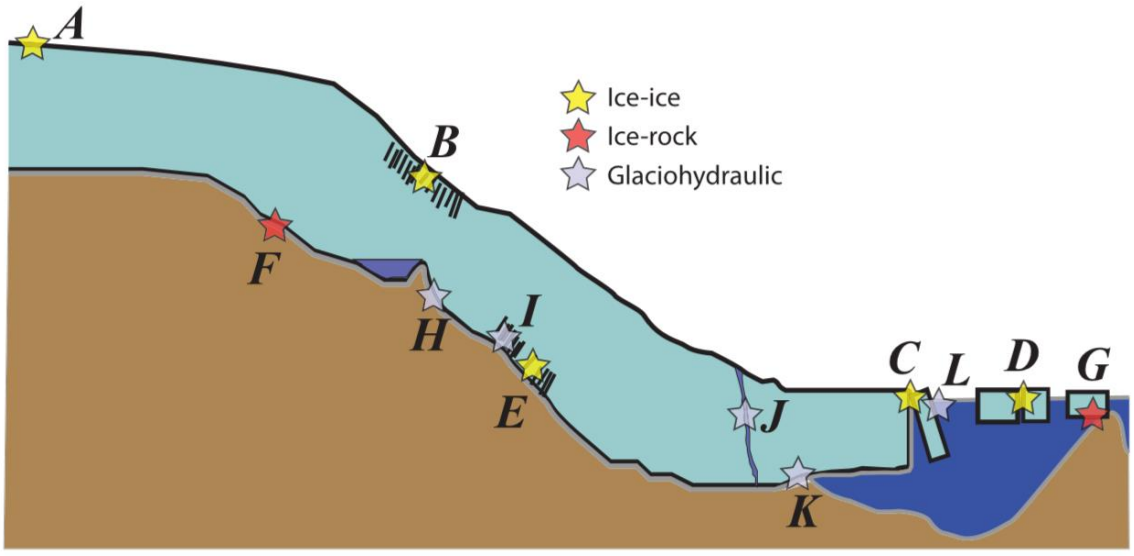

Figure 2. Schematic depiction of seismic source types (stars) in a glacial system from icecap to tidewater terminus. (A)–(E): sources associated with ice–ice dynamic processes; (A). Brittle icecap icequakes; (B). Surface crevasse opening or collapse (C). Calving; (D). Iceberg–iceberg collision, rifting, or fracture; (E). Basal crevasse opening or collapse. (F) and (G): Sources associated with ice-rock stick-slip; (F). Basal stick-slip; (G). Iceberg grounding. (H)–(L): Sources associated with ice-water interactions: (H). Subglacial lake drainage and transport; (I). Basal crevasse flow and resonance; (J). Moulin transport and tremor; (K). Terminus discharge; (L). Iceberg/Calving impact or other dynamic excitation of hydroacoustic, gravity, and seismic waves via the water column. [Reprinted from Aster and Winberry, 2017]

Numerous studies of cryoseismology and remote triggering of tectonic events are presented have been published since 2000, but only a few focus on or combine both fields [Podolskiy and Walter, 2016]. Peng et al. [2014] analyzed seismic stations in Antarctica during the 2010 Mw8.8 Maule earthquake in Chile. They identified clear high-frequency seismic signals (either local shallow icequakes or tectonic events) during or immediately after the passage of Rayleigh waves at several stations in Antarctica (e.g., YT.HOWD and ZM.AGO1). That study concluded that cryospheric systems in Antarctica could also be sensitive to large distant earthquakes. However, in many cases, triggered microseismicity was only recorded by a single or a few seismic stations because of sparse network distribution and data quality, making it challenging to locate the source and understand the triggering mechanism. In addition, only a few distant earthquakes (e.g., 2010 Chile earthquake and the 2011 Mw9.1 Tohoku-Oki earthquake) have been analyzed. Hence, it is hard to identify potential triggering threshold in selected regions.

CHAPTER 2. DATA AND METHODOLOGY

Here we conduct a systematic search for remotely triggered seismicity in Antarctica. We manage to examine many large distant earthquakes (Mw>8) with available and reasonable broadband data in Antarctica since 2000 for possible evidence of remote triggering by surface waves of remote events. To check the hypothesis that remote dynamic triggering phenomenon exists in many regions of Antarctica, we search for significant local seismicity increase during or immediately following surface waves. We analyze earthquake data recorded by various networks in Antarctica with detailed waveform analysis and visual inspection [Peng et al., 2014. Aiken and Peng, 2014. Bansal et al., 2016].

2.1 Broadband Data Sources

In this study, we utilize seismic data mostly from virtual network _ANTARCTICA (Antarctic Stations operating below 60 deg South) together with AI network (**Figures 3 and 4**), both downloaded from the IRIS Data Management Center (DMC), to identify remotely triggered seismicity after several significant events, including 2004 Mw9.1 Sumatra, 2010 Mw8.8 Maule, 2011 Mw9.1 Tohoku, 2012 Mw8.6 Indian Ocean, 2014 Mw8.2 Chile, 2015 Mw8.3 Chile and 2016 Mw7.8 Kaikoura earthquakes.

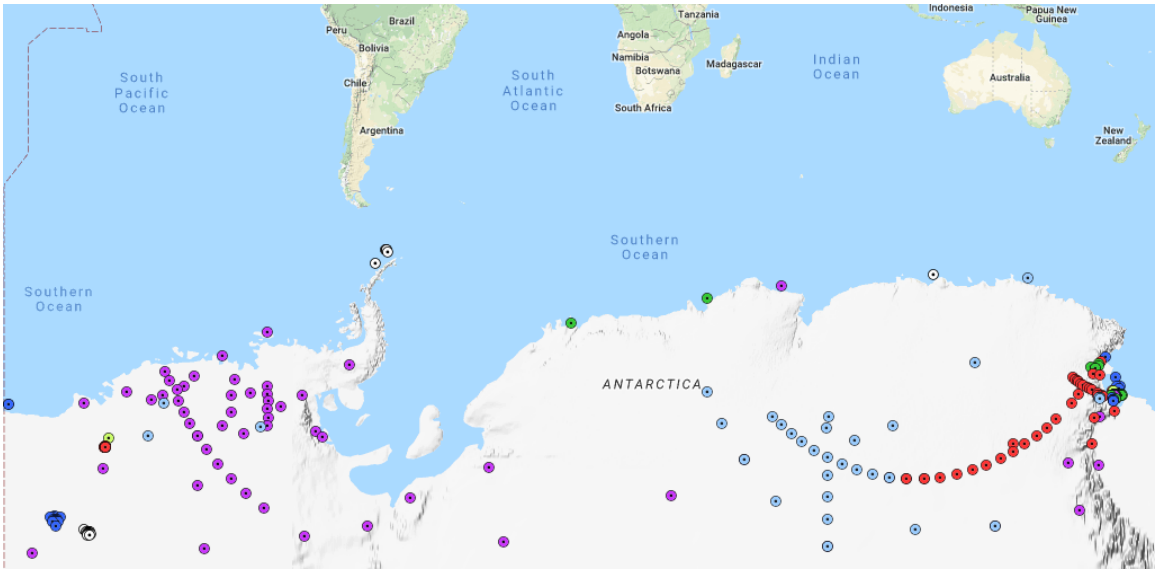

Figure 3. Location map of most stations (colored dots) in the virtual network _ANTARCTICA. 24 networks are identified by colors, in alphabetical order as AU, ER, G, GE, GT, IU (white), MN, PS, XA, XD, XI, XP (red), XU, XV (blue), Y4, YI, YT (purple), ZD, ZF, ZG, ZH, ZL, ZM (light blue) and ZW. Stations close to South Pole are not included.

Figure 4. Location map of all 6 stations (green dots) in AI network, in southward order as DSPA, ORCD, JUBA, JUBA, ESPZ, SMAI, BELA.

AI network, run by Argentina and Italy, fully operates with 6 permanent stations around Antarctica Peninsula and Scotia Plate since 2009. Benefited from modern instruments and lower elevation (9-262m), AI mostly provides high-quality broadband waveform data with low signal-noise ratio (SNR) and relatively lesser clipping effect.

As a virtual seismic network, _ANTARCTICA contains 364 stations and 24 networks in total spreading all over Antarctica but varies hugely in operation time scale and data quality. The oldest permanent station is ER.BOM on Mount Erebus with single-channel EHZ (extremely-short-period vertical channel) since 1981. The latest station is YT.MA09 in POLENET (Polar Earth Observing Network Project) mini-array, operating from 2015 till the end of 2016 with various channels.

Waveform data before 2007 (which is also the start year of POLENET) shares similar issues, such as low SNR, clipping, unpredictable section missing as well as varying availability. For example, only 9 stations' seismic records are accessible and feasible for waveform and spectrogram analysis during the 2004 Sumatra earthquake.

2.2 Waveform Analysis

In this study, we focus on whether and how local seismicity on Antarctica would be influenced by transient dynamic perturbations from surface waves of large distant earthquakes based on waveform & spectrogram analysis.

Surface waves are the largest amplitude signal from distant earthquakes as the energy decays with distance as 1/r. In contrast, body wave energy decays as $1/r^2$. Also, low-frequency components of surface waves from distant events (mostly lower than 5Hz) would dominate in seismograms, as compared to high-frequency components. However, for local seismic activities, seismic records on nearby stations are more dominated by high-

frequency signals (mainly higher than 5Hz, sometimes even extending over 10Hz), which could be utilized to differentiate local seismicity and distant events [Peng et al., 2014].

We first remove the instrument response to obtain broadband ground velocity with flat response mostly in 0.005-20 Hz. Broadband ground displacement could be obtained by integrating the velocity once. We also apply a 5 Hz high-pass filter to the instrument-corrected velocity records to identify and locate local seismic activities through time. Then apply the envelope function, which is essentially the amplitude of the Hilbert-transformed analytical signal, on the vertical component of high-pass-filtered seismic record several hours (typically 5 hours) before and after the mainshock P wave arrival time and shown in the log-based-10. If clear peaks could be identified during the passage of surface wave or right after, we zoom in around 1hr seismogram at the peak and retrospect to the raw three-component waveform. 5Hz high-pass-filter would still be applied on the raw waveform vertically. In order to inspect and detect high-frequency signals more clearly, we also compute the spectrogram on the vertical component as well. For most large distant events with consistent data, we follow the steps as mentioned above.

Waveform/spectrogram analysis and visual inspections both require reasonable SNR of seismic signal. High noise level and clipping effect would possibly dominate over the local seismicity change in the high-frequency field. However, the lack of existed stations in 2004 and the lack of quality data with high SNR, both bring difficulty in the same analysis process of the 2004 Sumatra earthquake. So, we simplify the process for the 2004 Sumatra earthquake by skipping the envelope function.

CHAPTER 3. RESULTS

After checking available broadband data on Antarctica, we have identified the 2010 Mw8.8 Maule, 2012 Mw8.6 Indian Ocean, 2016 Mw7.8 Kaikoura earthquakes as the distant large mainshocks highly possible triggered seismic activity at various stations on Antarctica. We also list two examples without triggering phenomenon as 2004 Sumatra and 2015 Chile for comparison.

3.1 2010 Mw8.8 Maule Earthquake

2010 Mw8.8 Maule earthquake is the most significant events in the Southern Hemisphere since the 1960 Mw9.5 Chile earthquake. Previous studies reveal that the 2010 Maule earthquake remotely triggered shallow earthquakes and deep tectonic tremor in central California, Cuba and New Zealand [Peng et al., 2010. Fry et al., 2011]. Also, the POLENET project started in 2007 with modern instruments and better data quality, which offers a great opportunity for the recording of possible remote triggering phenomenon.

Following the operation steps described in Chapter 2 and benefited from much better coverage of seismic networks on Antarctica, we examine more than 100 stations during the 2010 Maule earthquake and observe several stations with clear or possible remote triggering effect distributed over the continent. Most of the high-frequency signals emerge during and immediately after the passage of Rayleigh waves showing diverse patterns.

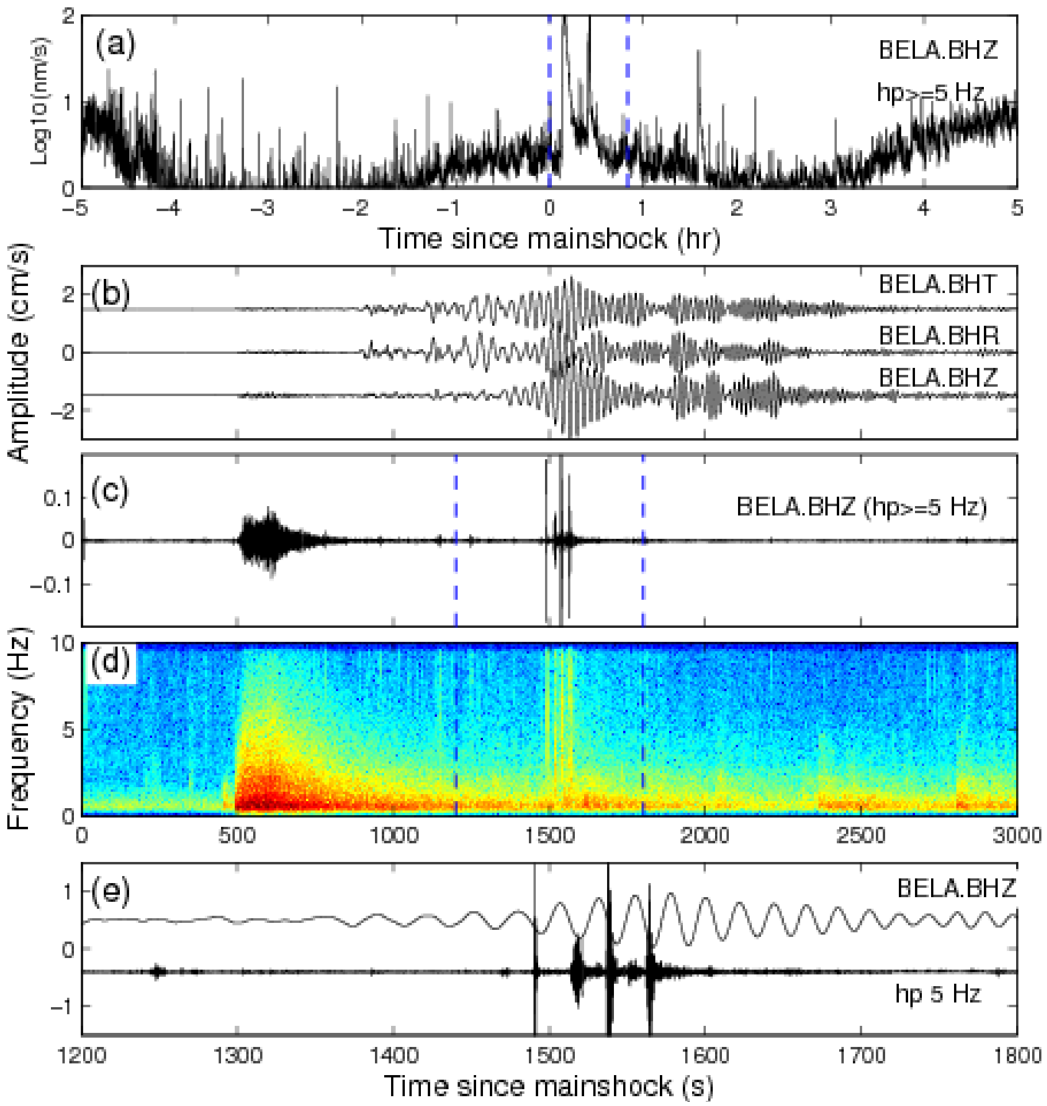

Figure 5. Station AI.BELA during 2010 Maule earthquake. Panel (a) Envelope function of 5Hz high-pass filtered waveform on the vertical component 5 hours before and after the mainshock. Dash line marks the peaks in 0-3000s. (b) Raw waveform in 0-3000s for three components. (c) 5Hz high-pass filtered in 0-3000s for vertical component. Dash line marks possible local seismicity. (d) 0-10Hz spectrogram in 0-3000s for vertical component. Dash line marks emerged high-frequency signal in 1200-1800s. (e) Possible triggered events during 1200-1800s shown as high-frequency signal emerges right on the passage of surface wave.

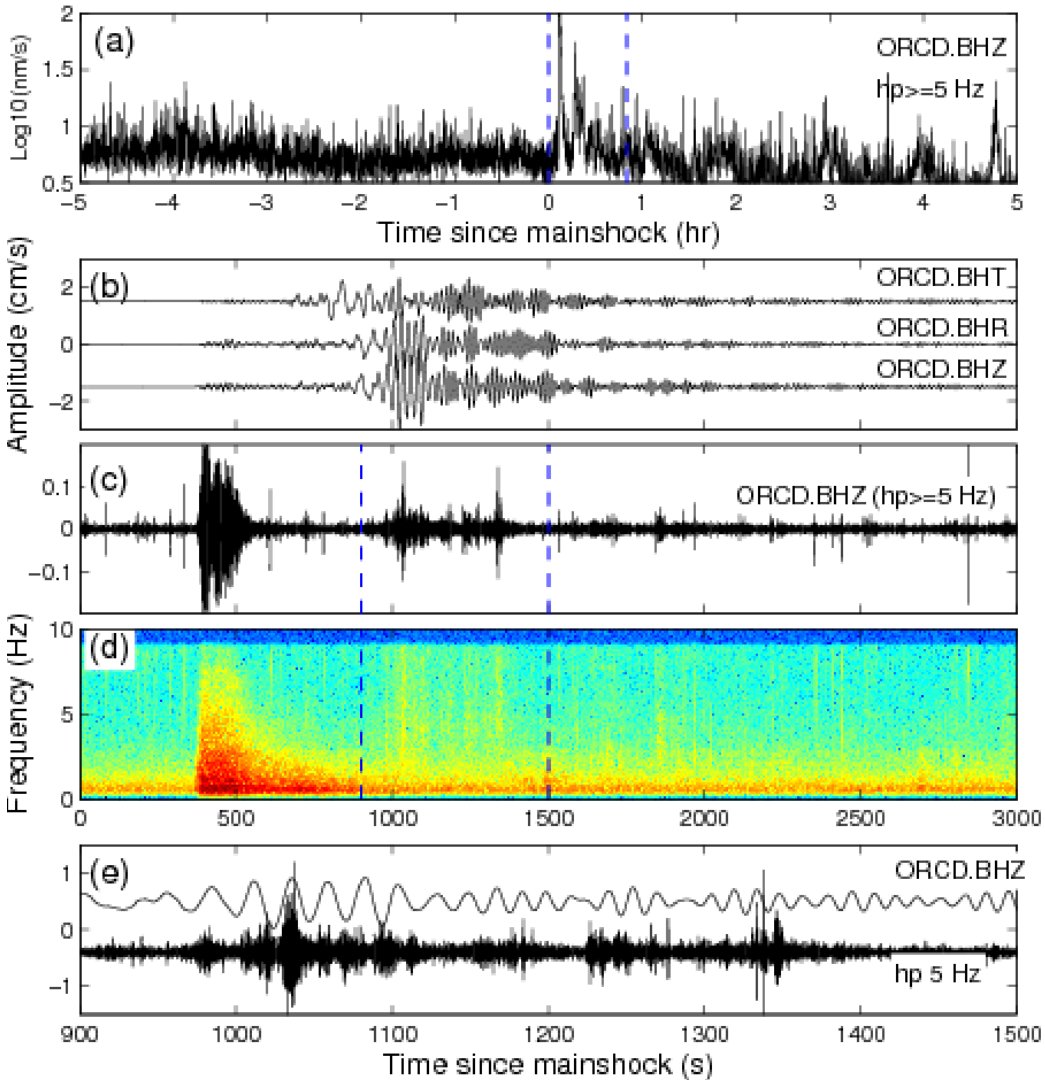

Figure 6. Station AI.ORCD during 2010 Maule earthquake. Panel (a) Envelope function of 5Hz high-pass filtered waveform on the vertical component 5 hours before and after the mainshock. Dash line marks the peaks in 0-3000s. (b) Raw waveform in 0-3000s for three components. (c) 5Hz high-pass filtered in 0-3000s for vertical component. Dash line marks possible local seismicity. (d) 0-10Hz spectrogram in 0-3000s for vertical component. Dash line marks emerged high-frequency signal in 900-1500s. (e) Possible triggered events during 900-1500s shown as high-frequency signal emerges right on the passage of surface wave.

As mentioned in 2.1, AI network provides acceptable seismic waveform data since 2009 as fully operated. We also observe clear evidence of high-frequency signals during 2010 Maule earthquakes on several stations of AI network (**Figures 5 and 6**). After the envelope function of 5Hz high-pass filtered waveform applied to the AI.BELA vertical component 5 hours before and after the mainshock, burst-like peaks of high-frequency signals occur in 0-3000s (**Figure 5a**). The corresponding unfiltered raw waveform indicates clear arrivals of P wave and Rayleigh wave (**Figure 5b**). The 5Hz high-pass filtered waveform and spectrogram show similar features: unexplained high-frequency signals emerge at the peak of the Rayleigh wave (**Figure 5c, d**). Then, we zoom in at the corresponding section of 1200-1800s. High-frequency signals correlate with the Rayleigh wave for ~100s, implying the local microseismicity triggered by distant surface waves. Station AI.ORCD also provides similar patterns as the high-frequency signals occur in 900-1500s, but correlate with original waveforms for much longer than BELA for ~500s.

Through both stations observe clear remotely triggering effect on the passage of Rayleigh waves, AI.ORCD shows relatively long-duration (~500s) high-frequency signals without clear P- or S- wave arrivals as normal and the high-pass filtered waveforms are coincident with the Rayleigh waves, suggesting that the possible triggered events are more tremor-like [Aiken et al. 2015]. In comparison, high-frequency signals at BELA last much shorter (~100s) with clear arrival peaks, implying that the burst-like signals refer to triggered seismic events.

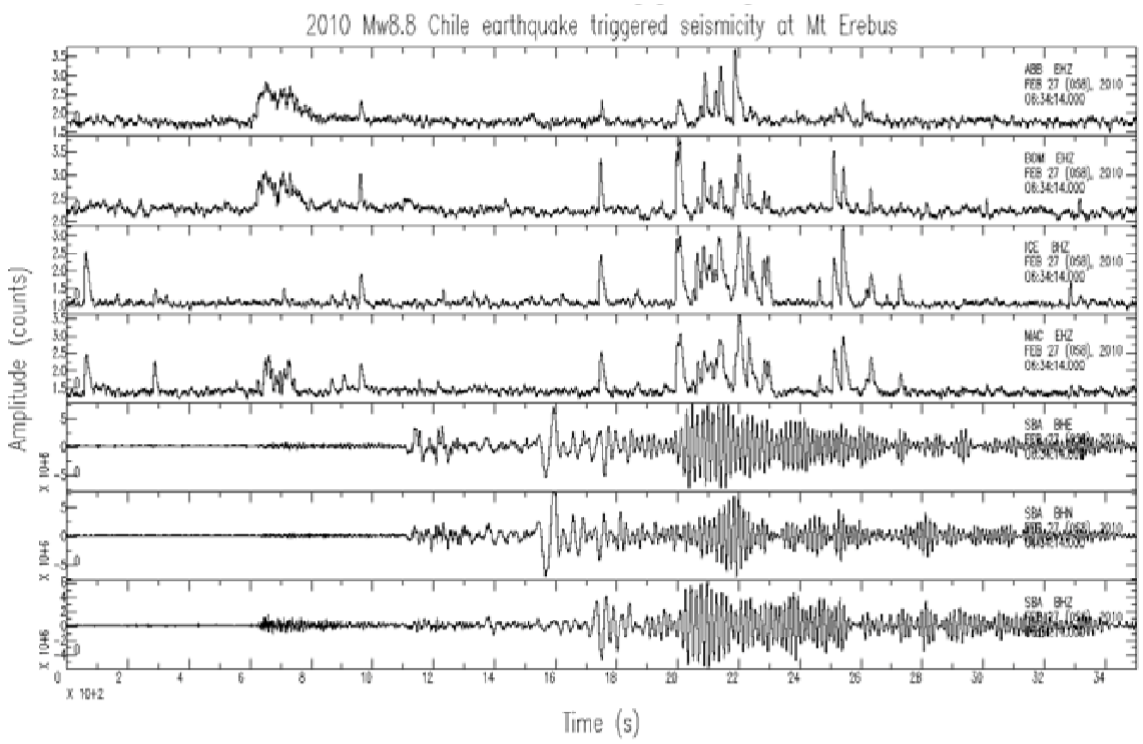

Figure 7. Possible triggered events at Mount Erebus following the 2010 Mw8.8 Maule earthquake (stations of ER.ABB, ER.BOM, ER.ICE, ER.MAC and IU.SBA). The top 4 traces show the envelope function (log10) of 5-Hz high-pass filtered vertical seismograms at 4 stations of ER network. The bottom 3 traces show the broadband velocity seismogram of a nearby station IU.SBA. High frequency spikes in the top 4 traces indicate possible triggering, mostly during the passage of Rayleigh waves.

Another possible remotely triggered example occurs at Mount Erebus following the 2010 Maule earthquake (**Figure 7**). As the southern-most active volcano on Earth, Mount Erebus is monitored by several seismic networks including temporary Y4, ZW, XV and permanent ER network [Aster et al., 2004]. After applying the envelope function log-base-

10 of 5Hz high-pass filter on the vertical seismic records at ER network, 4 stations (ABB, BOM, ICE, MAC) show clear high-frequency peaks at 2000-2600s. Unfiltered original broadband seismogram at IU.SBA (also at Mount Erebus but with a better quality record) shows that the high-frequency spikes emerge mostly on the passage of Rayleigh waves from 2010 Maule earthquake, which indicates possible remotely triggering effect at Mount Erebus area.

3.2 2012 Mw8.6 Indian Ocean Earthquake

The 2012 Mw8.6 Indian Ocean earthquake is the largest strike-slip event ever recorded. Previous study suggests that 2012 Indian Ocean earthquake triggered both magnitude >5.5 earthquakes around the world in the following weeks [Pollitz et al., 2012], as well as numerous deep tectonic tremor and microearthquakes in tectonically active regions in Asia [Wu et al., 2012; Wang et al., 2015; Chao and Obara, 2016; Li et al., 2019] and Africa [Neves et al., 2017]. It is worth noting that the Mw8.6 mainshock was followed by an Mw8.2 aftershock only 2 hours later.

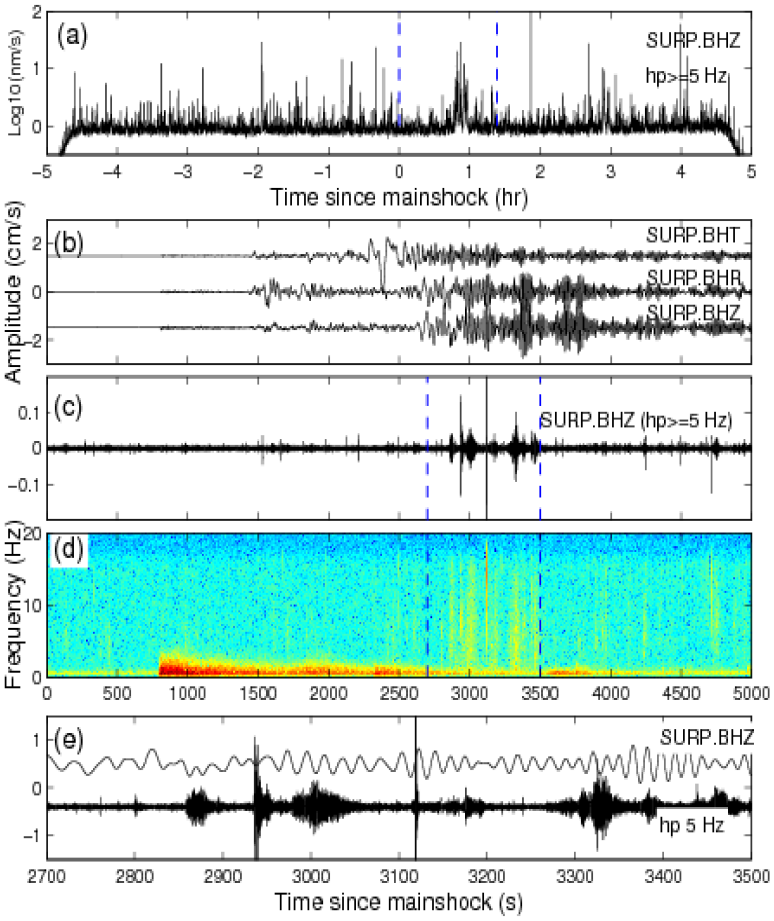

Figure 8. Station YT.SURP during 2012 Indian Ocean earthquake. Panel (a) Envelope function of 5Hz high-pass filtered waveform on the vertical component 5 hours before and after the mainshock. Dash line marks the peaks in 0-5000s. (b) Raw waveform in 0-5000s for three components. (c) 5Hz high-pass filtered in 0-5000s for vertical component. Dash line marks possible local seismicity. (d) 0-20Hz spectrogram in 0-5000s for vertical component. Dash line marks emerged high-frequency signal in 2700-3500s. (e) Possible triggered events during 2700-3500s shown as high-frequency signal emerges right on the passage of surface wave.

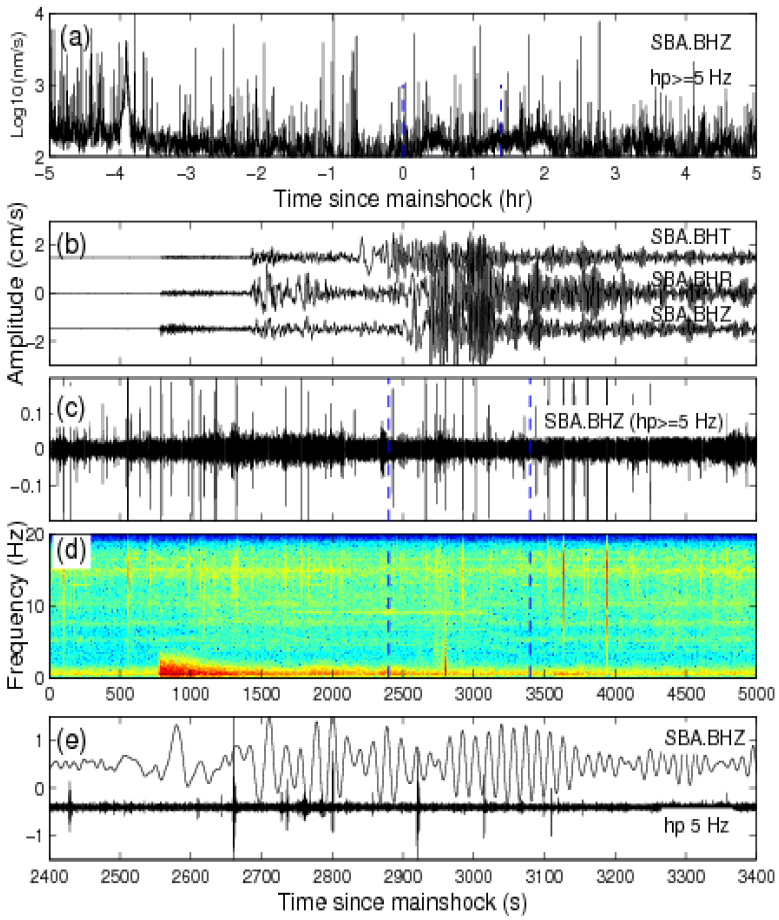

Figure 9. Station IU.SBA during 2012 Indian Ocean earthquake. Panel (a) Envelope function of 5Hz high-pass filtered waveform on the vertical component 5 hours before and after the mainshock. Dash line marks the peaks in 0-5000s. (b) Raw waveform in 0-5000s for three components. (c) 5Hz high-pass filtered in 0-5000s for vertical component. Dash line marks possible local seismicity. (d) 0-20Hz spectrogram in 0-5000s for vertical component. Dash line marks emerged high-frequency signal in 2400-3400s. (e) Possible triggered events during 2400-3400s shown as high-frequency signal emerges right on the passage of surface wave.

Here we take the station YT.SURP as the example of possible triggering evidence (**Figure 8**). Envelope function of 5Hz high-pass filtered waveform on the vertical component around the mainshock marks clear peak-like high-frequency around 1 hour and 3 hours region, respectively corresponding to the Mw8.6 mainshock and Mw8.2 aftershock. After evaluating the unfiltered original waveform record in 0-5000s, high-frequency signal occurs with the Rayleigh Wave around 2700-3500s, which could be clearly observed on the spectrogram as yellow stripes extended over 15 Hz. Correlation between raw seismogram and 5Hz high-pass filtered in 2700-3500 also implies that Rayleigh waves triggered local seismicity around YT.SURP station. Similar results are shown at station IU.SBA (**Figure 9**), but not as distinct as YT.SURP due to higher noise level and background activity as well as overlapping effect from the large aftershock.

3.3 2016 Mw7.8 Kaikoura Earthquake

Although under Mw8.0, we still take 2016 Mw7.8 Kaikoura earthquake into account for the relatively close distance and more available seismic data. One of the clear evidences of remote triggering effect is observed on station AU.MAW (**Figure 10**). High-frequency component appears at around 2300s, represented by the thick yellow stripes on the spectrogram and burst-like peak on envelope function as well as 5Hz high-pass filtered waveform at corresponding time region. The last panel (e) indicates that local microseismicity was triggered right after the passage of Rayleigh waves. Station IU.SBA gives comparable result (**Figure 11**), higher frequency emerging around 10Hz in 1000-1500s (yellow patch on the spectrogram). Also triggering effect occurs during the passage

of Rayleigh wave instead of after. With lower magnitude and energy, 2016 Kaikoura earthquake still triggers local seismicity on Antarctica for shorter duration ~100s.

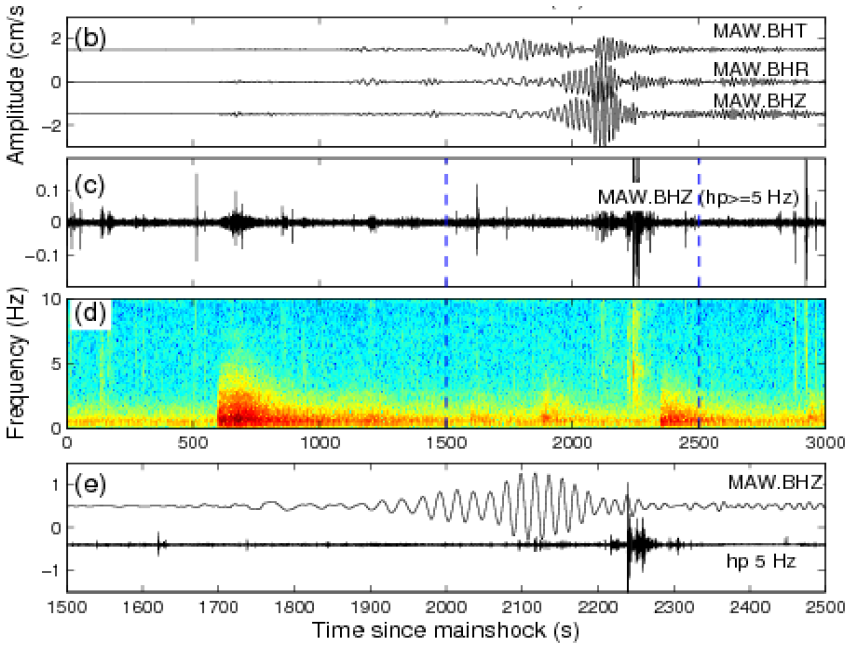

Figure 10. Station AU.MAW during 2016 Kaikoura earthquake. Panel (a) Envelope function of 5Hz high-pass filtered waveform on the vertical component 7500s before and 11000s after the mainshock. Red rectangle marks the peaks in 0-3000s. (b) Unfiltered waveform in 0-3000s for three components. (c) 5Hz high-pass filtered in 0-3000s for vertical component. Dash line marks possible local seismicity in 1500-2500s. (d) 0-10Hz spectrogram in 0-3000s for vertical component. Dash line marks emerged high-frequency signal in 1500-2500s. (e) Possible triggered events during 1500-2500s shown as high-frequency signal emerges right after the passage of surface wave.

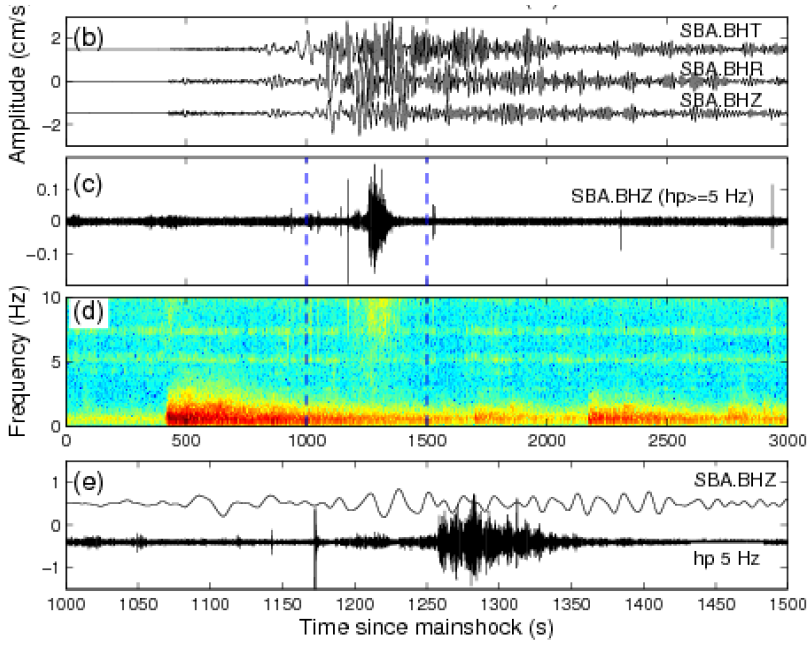

Figure 11. Station IU.SBA during 2016 Kaikoura earthquake. Panel (a) Envelope function of 5Hz high-pass filtered waveform on the vertical component 7500s before and 11000s after the mainshock. Red rectangle marks the peaks in 0-3000s. (b) Unfiltered waveform in 0-3000s for three components. (c) 5Hz high-pass filtered in 0-3000s for vertical component. Dash line marks possible local seismicity in 1000-1500s. (d) 0-10Hz spectrogram in 0-3000s for vertical component. Dash line marks emerged high-frequency signal in 1000-1500s. (e) Possible triggered events during 1000-1500s shown as high-frequency signal emerges right on the passage of surface wave.

3.4 2004 Mw9.1 Sumatra Earthquake (No clear triggering, T-phase)

For 2004 Mw9.1 Sumatra earthquake, only nine stations provide available open data for waveform & spectrogram analysis (AI.ORCD, AI.JUBA, IU.PMSA, IU.QSPA, IU.SBA, IU.CASY, GE.SNAA, PS.SYO, G.DRV) (**Figure 12a**). None of them show clear evidence of the possible remote triggering phenomenon. However, interestingly, three stations, SNAA, SYO and CASY (**Figure 12b**) show high-frequency signals on spectrograms, which should be more likely to be T-phase signal from Sumatra mainshock.

For the station GE.SNAA, we cut the vertical component of seismic record 15000s (~4 hours) before and after the 2004 Mw9.1 Sumatra mainshock (**Figure 13a**). The original seismogram is dominated by the Sumatra earthquake as expected. Then, we apply 2-8Hz band-pass filter and compute the spectrogram of 0-10Hz on the waveform (**Figure 13b, c**). Hours before mainshock, background activities existed around SNAA as several mild oscillations around -10000s to -5000s in panel(b), confirming the fact that border area is seismically active. In the spectrogram, although noisy, visible high-frequency signals emerge at 6000-10000s after the arrival of P- and S-waves, shown as the rectangle in panel(c). Similar signals could also be observed at PS.SYO and IU.CASY (**Figure 14, 15**), parallel high-frequency portion appears respectively at 5000-8000s and 4000-7000s. Station CASY gives the clearest high-frequency signals, which match the unreasonable peak and fluctuation in the corresponding panel(b) at same time region.

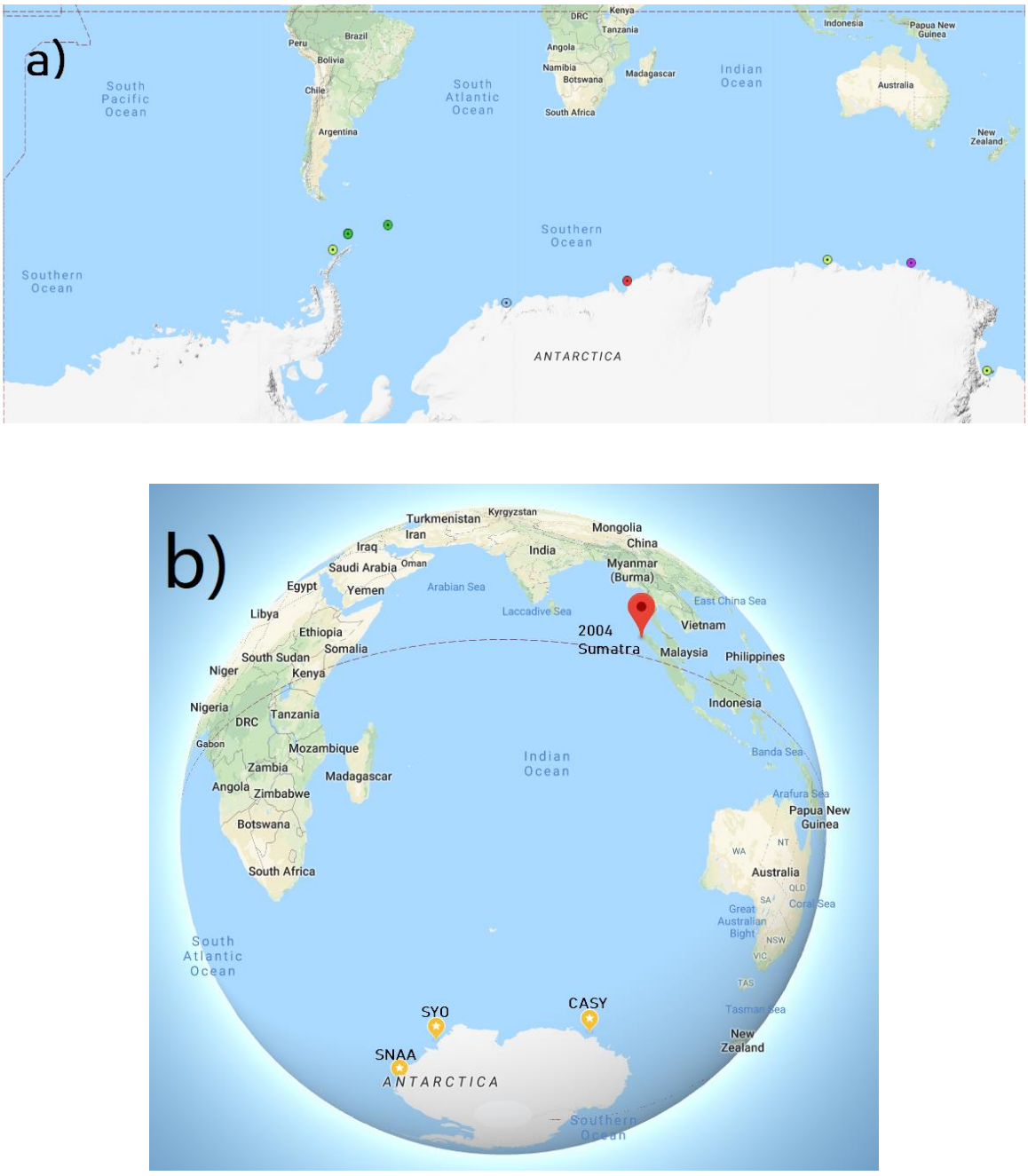

Figure 12. (a) Distribution of investigated stations, in eastward order as IU.PMSA, AI.JUBA, AI.ORCD, GE.SNAA, PS.SYO, IU.CASY, G.DRV, IU.SBA. Station IU.QSPA locates at the South Pole, which could not be seen in Mercator plot. **(b)**Relatively location map between stations (yellow stars) as GE.SNAA, PS.SYO and IU.CASY relative to the 2004 Mw9.1 Sumatra earthquake (red).

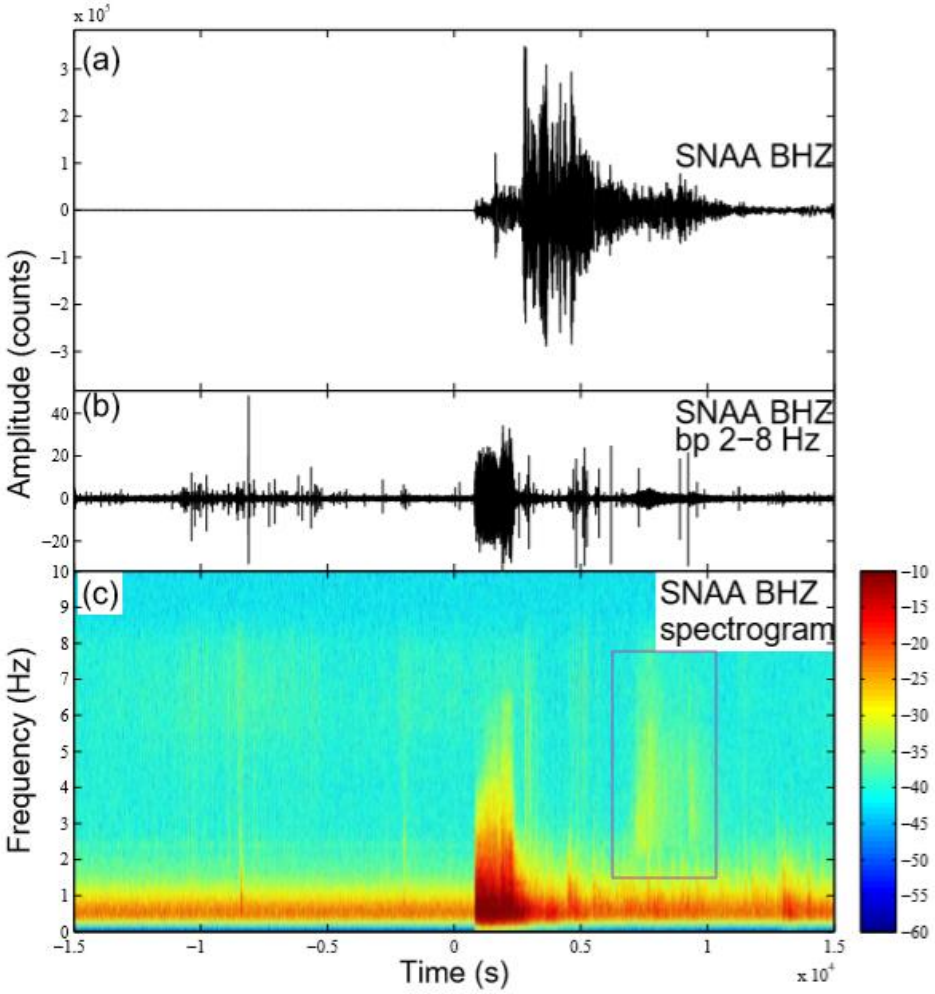

Figure 13. Station GE.SNAA during 2004 Sumatra earthquake. Panel (a): Original vertical broadband waveform data 15000s (~4 hours) before and after the mainshock. (b): 2-8Hz bandpass filtered waveform. (c) Spectrogram in 0-10Hz. Rectangle marks the emerged high-frequency signal on the passage of Rayleigh wave at 6000-10000s.

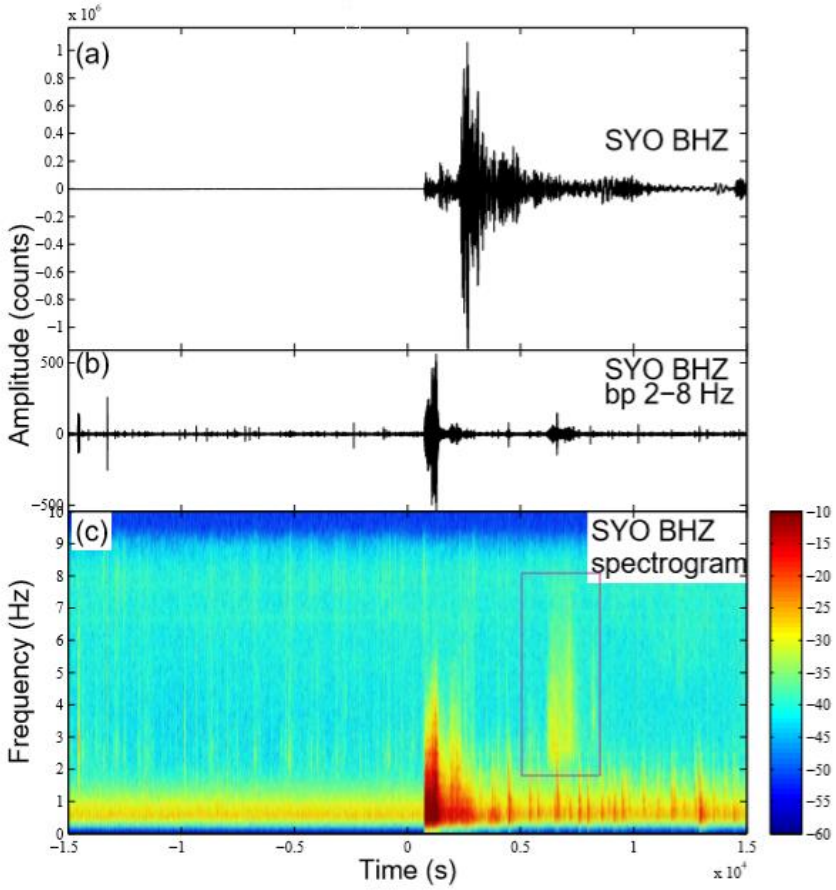

Figure 14. Station PS.SYO during 2004 Sumatra earthquake. Panel (a): Original vertical broadband waveform data 15000s (~4 hours) before and after the mainshock. (b): 2-8Hz bandpass filtered waveform. (c) Spectrogram in 0-10Hz. Rectangle marks the emerged high-frequency signal on the passage of Rayleigh wave at 5000-8000s.

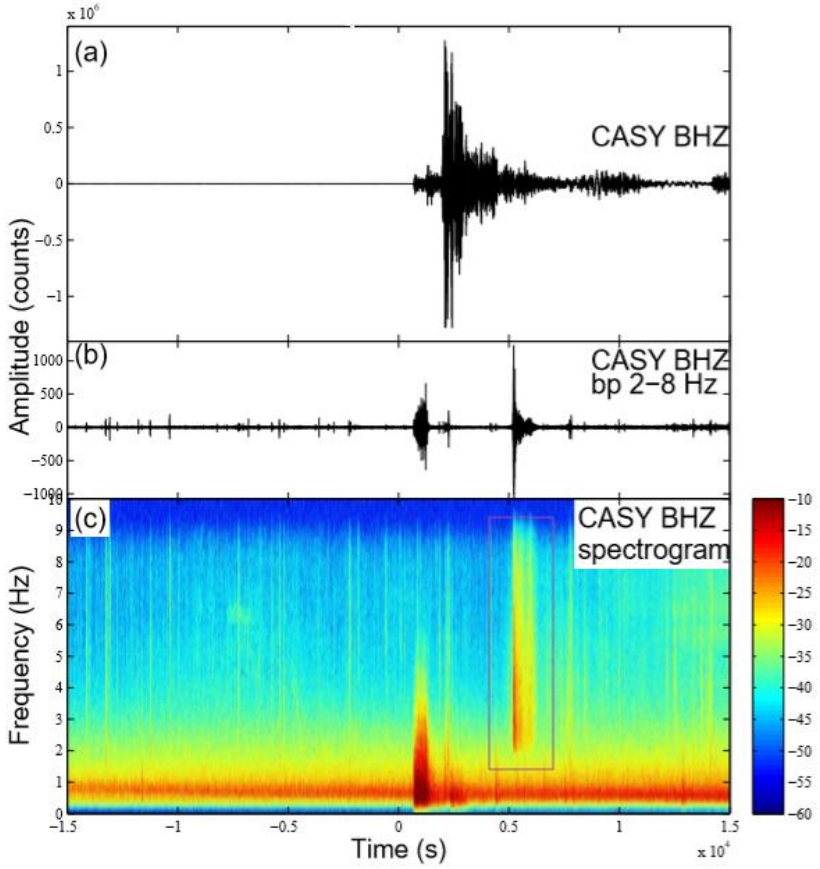

Figure 15. Station IU.CASY during 2004 Sumatra earthquake. Panel (a): Original vertical broadband waveform data 15000s (~4 hours) before and after the mainshock. (b): 2-8Hz bandpass filtered waveform. (c) Spectrogram in 0-10Hz. Rectangle marks the emerged high-frequency signal on the passage of Rayleigh wave at 4000-7000s.

Table 1. Estimation on arrival time of T-phase for Sumatra earthquakes at three stations GE.SNAA, PS.SYO and IU.CASY, as compared to the actual emergence time of high-frequency signal on spectrograms.

	GE.SNAA 11625km	PS.SYO 10180km	IU.CASY 8750km
Estimation from T-phase	7750s	6787s	5833s
Actual emergence time of high-frequency	~7500s	~6500s	~5500s

Here, much higher frequency and intensity than background activity/noise level indicate probable T-phase from Sumatra mainshock instead of triggering effect. As recorded similarly by three stations, high-frequency signals (~2-8Hz) last for ~700s with an apparent absence of lower frequency. The band-pass filtered waveforms (panel (b) of **Figures 13, 14, 15**) show no evidence of the arrival of P-, S- and surface waves from possible local triggered events. Instead, the clear single peak in the same time region refers to the arrival of particular waves. Previous studies suggest that T-phase or T-wave derives from deep-ocean earthquakes. At a velocity around 1.5km/s, T-phase could be observed on

spectrogram in the high-frequency domain (1-35Hz) with considerable spectral length, and typically correlate with the seismic moments [Ewing et al., 1952. Walker et al., 1992]. We conduct a simple estimation based on the distance from epicenter in **Table S1** for the arrival time at three stations. The result matches with the spectrogram. The similarity between the last time of high-frequency signal (~700s) and the rupture time of the 2004 Sumatra earthquake (600-650s) also suggests T-phase instead of remote triggering effect.

It is worth noting that the IU.QSPA station provided the highest SNR record, when the 2004 Sumatra earthquake happened, which could be verified on the relevant spectrogram (**Figure 16**). Known as South Pole Remote Earth Science Observatory (Quiet Zone), station IU.QSPA locates 8 km from the geographic South Pole and sits on a glacier about 2.5km thick. From the seismogram and spectrogram, QSPA remains extremely quiet before the arriving of teleseismic P waves from the Sumatra mainshock. Due to the enormous magnitude of Sumatra earthquake, the input seismic signals exceeded the acceptable range of seismometer for several seconds and resulted in apparent clipping effect on the record. On and after the passage of surface waves, no high-frequency seismic signals emerged, suggesting no triggered events around the South Pole during the 2004 Sumatra earthquake.

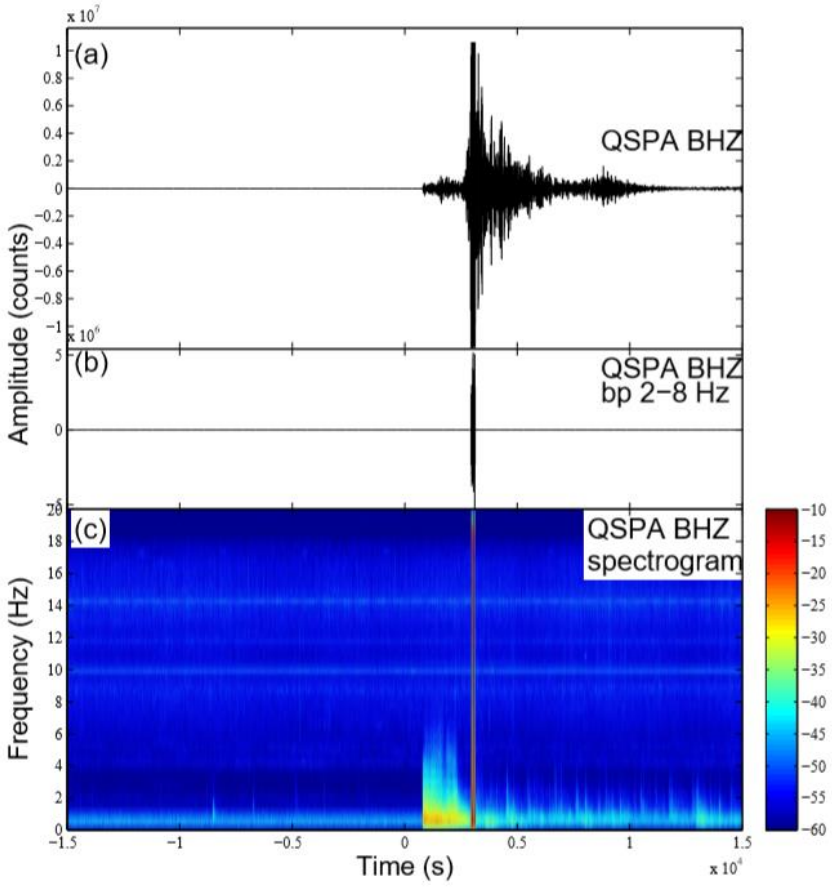

Figure 16. Station IU.QSPA during 2004 Sumatra earthquake. Panel (a): Original vertical broadband waveform data 15000s (~4 hours) before and after the mainshock. (b): 2-8Hz bandpass filtered waveform. (c) Spectrogram in 0-20Hz. Clear clipping effect shown as single vertical stripe.

3.5 2015 Mw8.3 Chile Earthquake (No triggering)

Last, we introduce another none-triggering example as 2015 Mw8.3 Chile earthquake at station ER.HOO (**Figure 17**). Compared to the 2010 Mw8.8 Maule earthquake, there are no abnormal peaks during or after the passage of surface waves on the envelope function of 5Hz high-pass filtered. Instead, multiple peaks distribute through the 10 hours record before and after the mainshock with various amplitude, implying high intensity of local seismicity and probably noise. Also, no clear high-frequency patch or stripe exists on the spectrogram in the relevant time region. Patterns refer to none apparent triggering effect at ER.HOO during 2015 Chile earthquake.

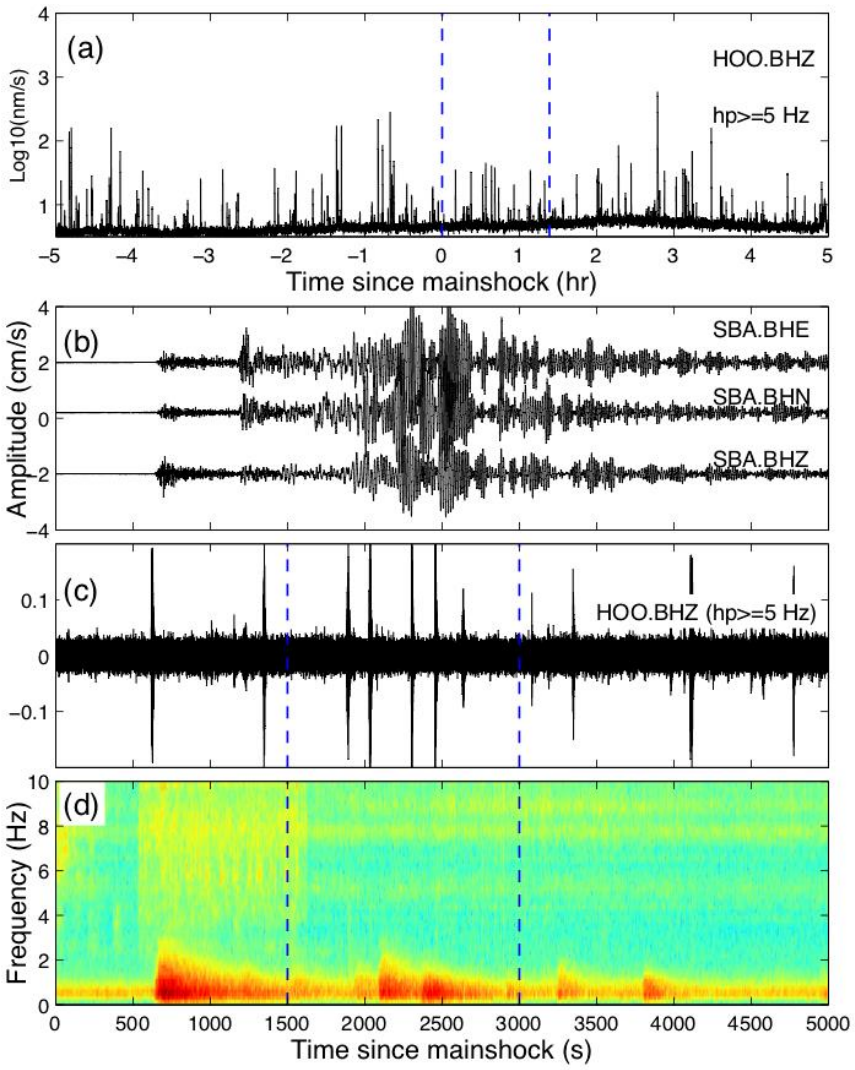

Figure 17. Mount Erebus network ER and station IU.SBA during 2015 Chile earthquake. Panel (a) Envelope function of 5Hz high-pass filtered waveform on the vertical component 5 hours before and after the mainshock on station ER.HOO. Dash line marks the peaks in 0-5000s. (b) Unfiltered waveform on station IU.SBA in 0-5000s for three components. (c) 5Hz high-pass filtered in 0-5000s for vertical component of ER.HOO. Dash line marks possible local seismicity in 1500-3000s. (d) 0-10Hz spectrogram in 0-5000s for vertical component. No clear high-frequency signal emerges in corresponding time region.

CHAPTER 4. DISCUSSION

4.1 Dynamic Stress Change

We estimate the dynamic stress change using the observed peak ground velocity (PGV) at station IU.SBA, a shear rigidity (μ) of 30GPa and surface-wave phase velocities (V_{ph}) of 4.0km/s and 3.0km/s for the Love and Rayleigh waves as following,

$$\sigma = \frac{(PGV)(\mu)}{Vph}$$ [Hill and Prejean, 2015]

As one of the few stations that keeps stable records continuously through our research time scale, IU.SBA station has operated continuously since 1998-10-28 with twice instruments update in 2009 and 2014. IU.SBA locates close to the Scott base and US's Antarctica McMurdo Station near Mount Erebus on Ross Island. Mount Erebus is a large active stratovolcano with ongoing small-scale eruptions and existing monitoring infrastructures, making it more sensitive to dynamic stress change affected by surface waves from distant large earthquakes.

We conduct the calculation at one station IU.SBA through most significant events (Mw>5.5) since 2000. Then, we sort out and figure those with dynamic stress higher than 1kpa (**Figure 18**). To make figures more comprehensive, we also pick several events with lower stress change (between 0.1KPa to 1KPa) after visual inspection of no triggering phenomenon, and combine them into the figure. It is worth mentioning that every event shown in **Figure 18** is larger than Mw6.5.

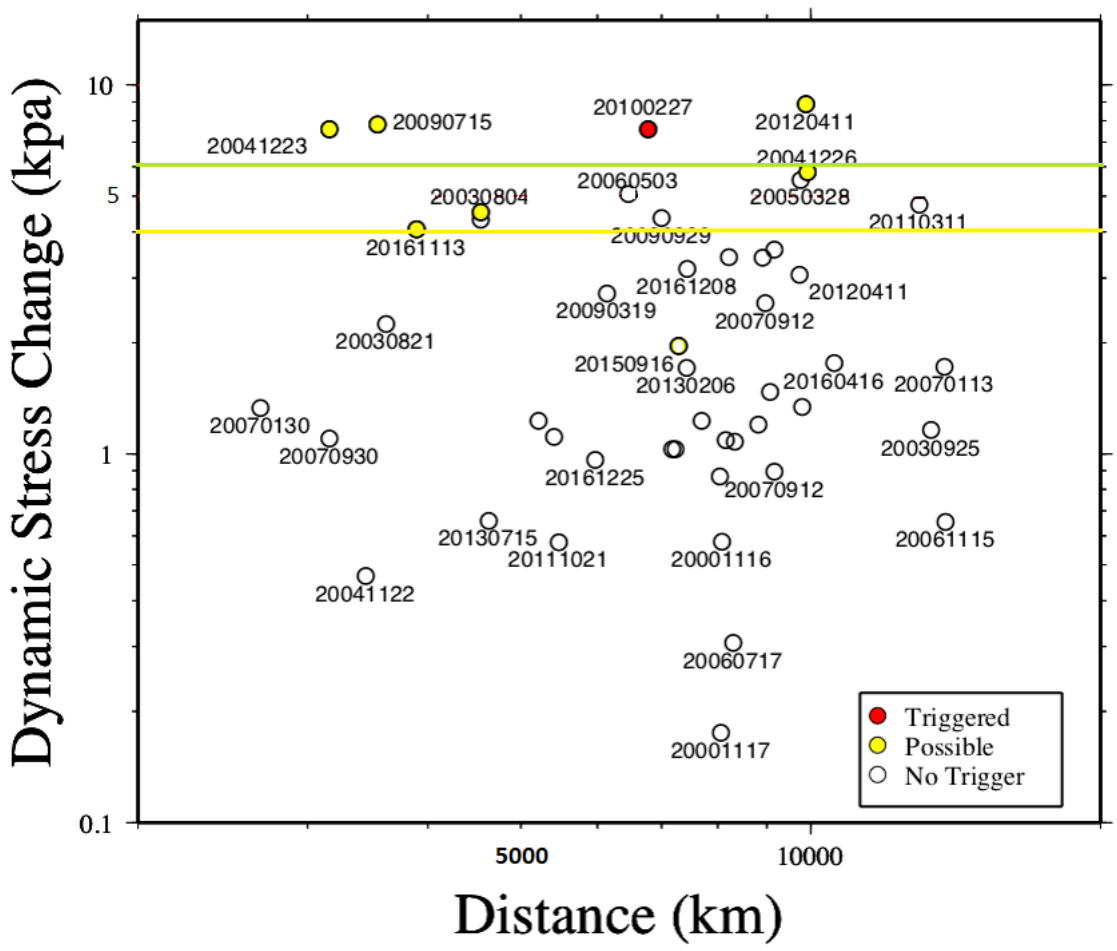

Figure 18. Dynamic stress change and distance at station IU.SBA, calculated from peak ground velocity (PGV). The events with clear evidence of triggering and potential triggering are marked as red and yellow circles. Triggering threshold are marked as solid lines, 4 KPa (yellow line) as possible threshold and 6 KPa (green line) as positive threshold.

For most mainshocks, dynamic stress change estimations at IU.SBA under 5kpa show no triggering effect. Generally, more intense dynamic stress change would be more likely to trigger local seismicity. If dynamic stress change reaches 4KPa (yellow line in **Figure 18)**, possible triggering effect could be observed. Every mainshock with 6KPa or higher (green line in **Figure 18)** dynamic stress change will trigger local events in Antarctica. Maximal dynamic stress values are ~8KPa for 2010 Maule earthquake and ~9KPa for 2012 Indian Ocean earthquake. Both are shown clear evidence of possible remotely triggering effect on or right after the passage of Rayleigh waves. Dynamic triggering thresholds are likely site-, time- and frequency-dependent [Hill and Prejean, 2015]. Previous studies show that generally, most thresholds stay around 5-10 KPa, as high as ~40KPa and as low as ~1KPa. Our results coincide with the threshold of 4-6KPa marked in the figure, which imply that similar dynamic triggering effect could also happen on Antarctica for similar mechanisms and could be investigated with similar methods.

4.2 Spatial Distribution of Triggering Sites

In the most general terms, Antarctica could be divided into three major areas: West Antarctica, East Antarctica and the Antarctic Peninsula (**Figure 19**). The Antarctic Peninsula has many glaciers and floating ice shelves that are changing rapidly as this part of Antarctica is warming faster than the rest of the continent. Also, the terminal of the Antarctic Peninsula is connected with the boundary of Antarctic Plate and several active minor tectonic plates, such as Scotia Plate and South Sandwich Plate. Along the peninsula are the Transantarctic Mountains, extending across the continent and separating East and

West Antarctica. East Antarctica is considerably larger with thicker ice sheet and more stable than West Antarctica. The glacier flows much intensively in West Antarctica as the lower elevation of bedrock makes the interaction between ice bottom and ocean water more feasible.

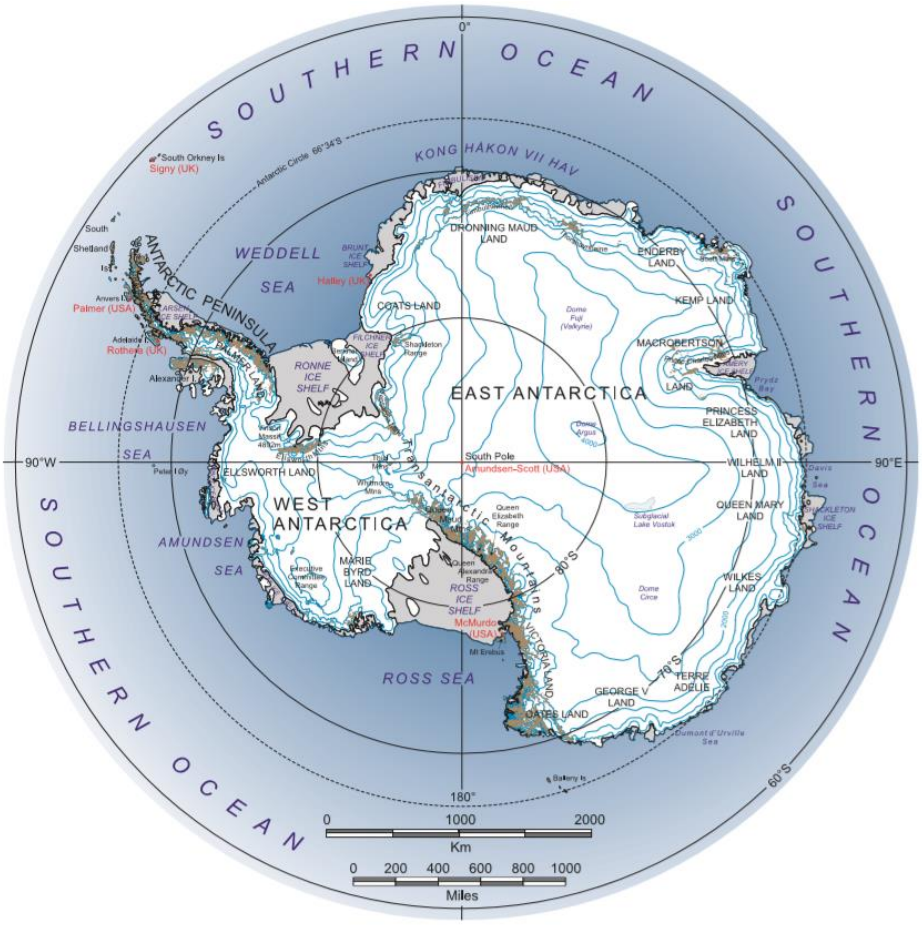

Figure 19. Antarctica overview map with major geographical features. [Reprinted from the British Antarctic Survey website]

The tectonic and glacier movement background coincide with the possible remotely triggering effect distribution (**Figure 20**). Most evidence of triggering occurs on West Antarctica and Antarctic Peninsula, while the heartland of East Antarctica remains quiet and none triggered. Our results are consistent with previous studies [Peng et al., 2014]. Besides, the phenomenon that many possible triggered stations are located along the coast of Antarctica, results from more interaction between the ice sheet and oceans, and much closer to the plate boundary. Thus, the coast area is prone to at the critical state and remotely triggered. Stations and networks on the rim of Antarctica would be more convenient to install and maintain, which results in better data quality. Surface waves traveled directly through oceans with less decay and higher amplitude when arriving at these stations. Higher dynamic stress change also contributes to the remote triggering effect. It is worth noting that Mount Erebus has been regarded as the most tectonically active area on Antarctica with several detected possible triggered events through 2010 Maule earthquake (**Figure 21**).

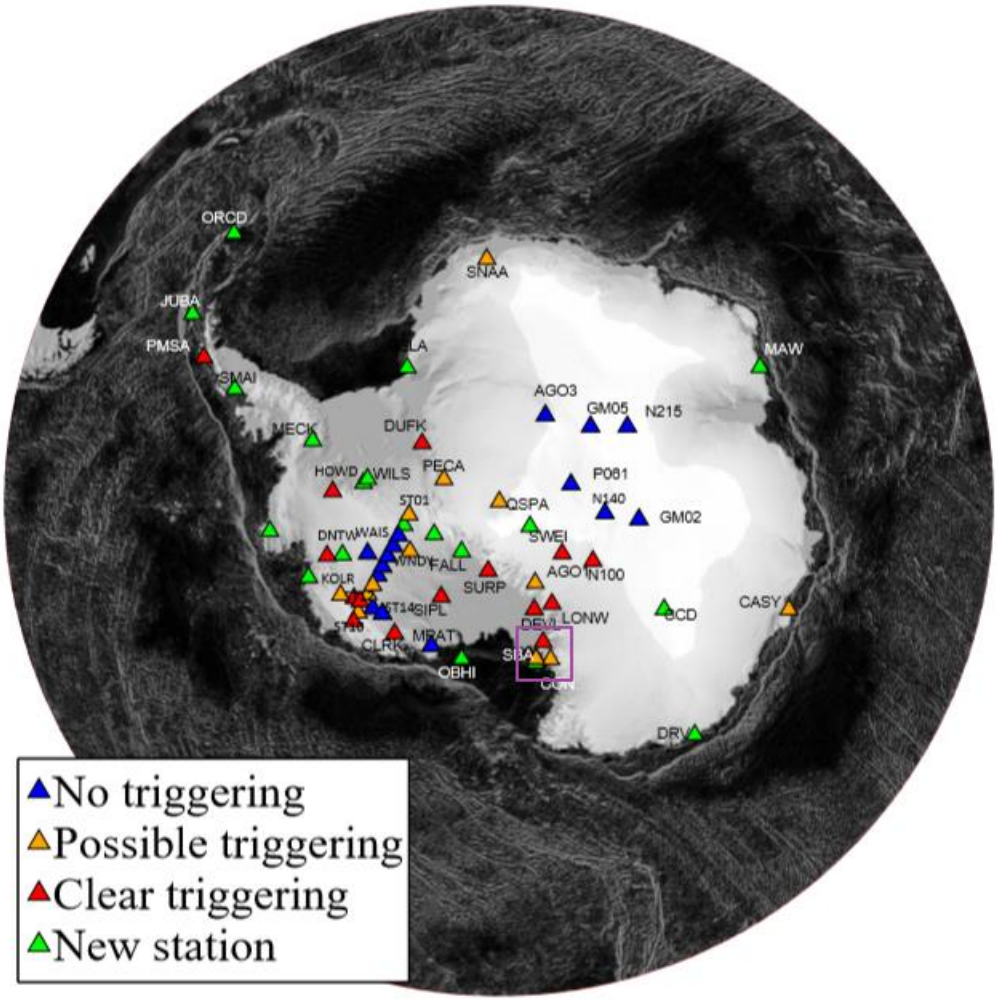

Figure 20. Map of Antarctica and surrounding regions indicating seismic stations with clear (red), possible (orange and green), and no (blue) triggering during the passage of 2010 Mw8.8 Maule, Chile mainshock surface waves. Purple box refers to Mount Erebus area (**Figure 20**). New stations indicate newly found seismic stations with possible remote triggered effect compared to the previous study [Peng et al., 2014].

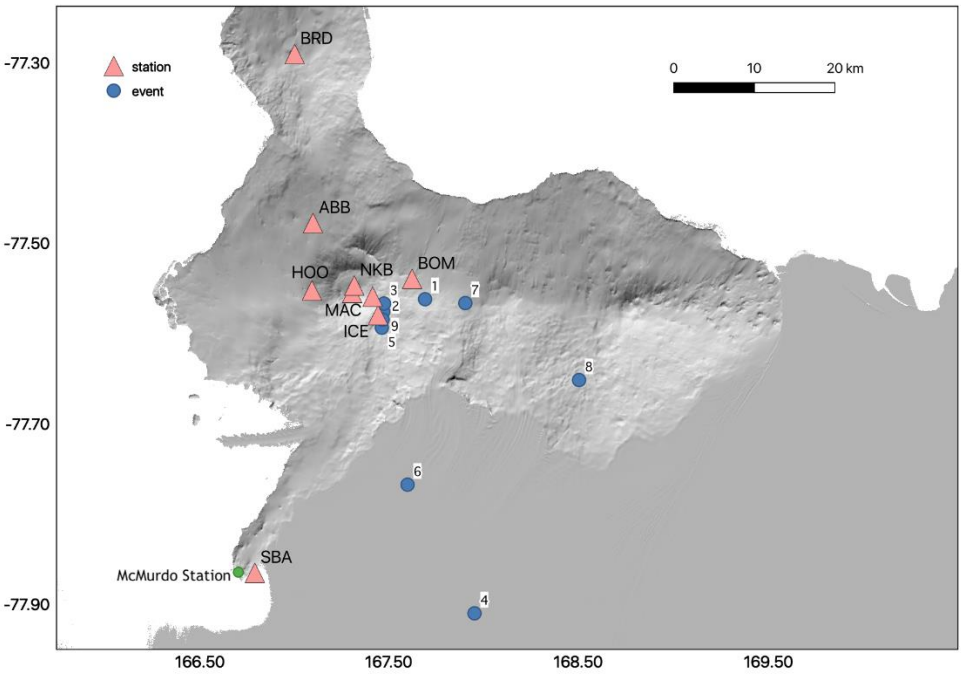

Figure 21. Map of Mount Erebus and stations used in the study. Blue circles are detected triggered events during surface waves of 2010 Mw8.8 Maule earthquake with matched-filter methods. [Peng et al., 2019]

CHAPTER 5. CONCLUSIONS

Identifying the remotely triggering effect by distant significant global earthquakes on Antarctica has barely been attempted previously. As an extension of the 2014 Nature Geoscience work [Peng et al., 2014], results presented in this study show that multiple large earthquakes since 2000 possibly triggered local seismicity at various locations in Antarctica. These include the 2010 Mw8.8 Maule, 2012 Mw8.6 Indian Ocean and 2016 Mw7.8 Kaikoura earthquakes. The possible triggering effect varies between events and targeted stations, but mainly follows similar patterns: local microseismicity represented by the abnormal high-frequency signal on waveform and spectrogram emerges on or right after the passage of Rayleigh waves from distant events. Depend on the size of mainshocks and triggered events, local high-frequency signals would last from 100s to over 500s and vary from 5Hz to over 15Hz. Most of the triggered local events could only be recorded on a single station owing to the tiny size and sparse distribution of networks. Besides, estimations on the dynamic stress change on IU.SBA through events since 2000 corroborates the possible simplified criterion of remote triggering as the stress threshold of 5kpa. Last, we also found that the distribution of possible triggered stations/locations fits with the Antarctica tectonic background well, as most evidences of triggering occur on West Antarctica and Antarctic Peninsula.

Future work is expected to employ more systematic method and better data processing plan. Our next step on this project is to detect more seismic or aseismic events throughout Antarctica to complete the primary seismicity distribution map. Matched filter analysis or deep-learning method would help to utilize all available seismic record and

boost the relocation work. The comparison between seismicity change before and after the large distant earthquakes could also contribute to the study of regional triggering sensitivity. We believe that these problems demonstrate the need for systematic analysis on Antarctica that might lead to a better understanding of the triggered source mechanisms and potential spatio-temporal relationship, the interaction among global earthquakes, glacier movement and Antarctic tectonic background.

REFERENCES

[1] Aiken, C., Peng, Z., & Chao, K. (2013). Tremors along the Queen Charlotte Margin triggered by large teleseismic earthquakes. *Geophysical Research Letters*, *40*(5), 829-834.

[2] Aiken, C., & Peng, Z. (2014). Dynamic triggering of microearthquakes in three geothermal/volcanic regions of California. *Journal of Geophysical Research: Solid Earth*, *119*(9), 6992-7009.

[3] Aiken, C., Zimmerman, J. P., Peng, Z., & Walter, J. I. (2015). Triggered seismic events along the eastern Denali fault in northwest Canada following the 2012 M w 7.8 Haida Gwaii, 2013 M w 7.5 Craig, and two M w> 8.5 teleseismic earthquakes. *Bulletin of the Seismological Society of America*, *105*(2B), 1165-1177.

[4] Aron, A., & Hardebeck, J. L. (2009). Seismicity rate changes along the central California coast due to stress changes from the 2003 M 6.5 San Simeon and 2004 M 6.0 Parkfield earthquakes. *Bulletin of the Seismological Society of America*, *99*(4), 2280-2292.

[5] Aster, R., MacIntosh, W., Kyle, P., Esser, R., Bartel, B., Dunbar, N., Johnson J, Karstens R, Kurnik C, McGowan M, McNamara, S. (2004). Real-time data received from Mount Erebus volcano, Antarctica. *Eos, Transactions American Geophysical Union*, *85*(10), 97-101.

[6] Aster, R. C., & Winberry, J. P. (2017). Glacial seismology. *Reports on Progress in Physics*, *80*(12), 126801.

[7] Bansal, A. R., Yao, D., Peng, Z., & Sianipar, D. (2016). Isolated regions of remote triggering in South/Southeast Asia following the 2012 Mw 8.6 Indian Ocean earthquake. *Geophysical Research Letters*, *43*(20), 10-654.

[8] Chao, K., & Obara, K. (2016). Triggered tectonic tremor in various types of fault systems of Japan following the 2012 Mw8. 6 Sumatra earthquake. *Journal of Geophysical Research: Solid Earth*, *121*(1), 170-187.

[9] Ewing, M., Press, F., & Worzel, J. L. (1952). Further study of the T phase. *Bulletin of the Seismological Society of America*, *42*(1), 37-51.

[10] Fry, B., Chao, K., Bannister, S., Peng, Z., & Wallace, L. (2011). Deep tremor in New Zealand triggered by the 2010 Mw8. 8 Chile earthquake. *Geophysical Research Letters*, *38*(15).

[11] Gomberg, J., Reasenberg, P. A., Bodin, P. L., & Harris, R. A. (2001). Earthquake triggering by seismic waves following the Landers and Hector Mine earthquakes. *Nature*, *411*(6836), 462.

[12] Gomberg, J., Bodin, P., Larson, K., & Dragert, H. (2004). Earthquake nucleation by transient deformations caused by the M= 7.9 Denali, Alaska, earthquake. *Nature*, *427*(6975), 621.

[13] Hill, D. P., Reasenberg, P. A., Michael, A., Arabaz, W. J., Beroza, G., Brumbaugh, D., Brune, J. N., Castro, R., Davis, S., dePolo, D.& Ellsworth, W. L. (1993). Seismicity remotely triggered by the magnitude 7.3 Landers, California, earthquake. *Science*, *260*(5114), 1617-1623.

[14] Hill, D. P. (2008). Dynamic stresses, Coulomb failure, and remote triggering. *Bulletin of the Seismological Society of America*, *98*(1), 66-92.

[15] Hill, D. P. (2012). Surface-wave potential for triggering tectonic (nonvolcanic) tremor—Corrected. *Bulletin of the Seismological Society of America*, *102*(6), 2337-2355.

[16] Hill, D. P., & Prejean, S. (2015). Dynamic triggering, 273-304.

[17] Johnson, P. A., Savage, H., Knuth, M., Gomberg, J., & Marone, C. (2008). Effects of acoustic waves on stick–slip in granular media and implications for earthquakes. *Nature*, *451*(7174), 57.

[18] Lay, T. (2015). The surge of great earthquakes from 2004 to 2014. *Earth and Planetary Science Letters*, *409*, 133-146.

[19] Li, L., Wang, B., Peng, Z., & Li, D. (2019). Dynamic triggering of microseismicity in Southwest China following the 2004 Sumatra and 2012 Indian Ocean earthquakes. *Journal of Asian Earth Sciences*, *176*, 129-140.

[20] Lough, A. C., Wiens, D. A., & Nyblade, A. (2018). Reactivation of ancient Antarctic rift zones by intraplate seismicity. *Nature Geoscience*, *11*(7), 515.

[21] Neves, M., Custódio, S., Peng, Z., & Ayorinde, A. (2017). Earthquake triggering in southeast Africa following the 2012 Indian Ocean earthquake. *Geophysical Journal International*, *212*(2), 1331-1343.

[22] Okal, E. A. (1981). Intraplate seismicity of Antarctica and tectonic implications. *Earth and planetary science letters*, *52*(2), 397-409.

[23] Peng, Z., & Gomberg, J. (2010). An integrated perspective of the continuum between earthquakes and slow-slip phenomena. *Nature geoscience*, *3*(9), 599.

[24] Peng, Z., Hill, D. P., Shelly, D. R., & Aiken, C. (2010). Remotely triggered microearthquakes and tremor in central California following the 2010 Mw 8.8 Chile earthquake. *Geophysical Research Letters*, *37*(24).

[25] Peng, Z., Gonzalez-Huizar, H., Chao, K., Aiken, C., Moreno, B., & Armstrong, G. (2013). Tectonic tremor beneath Cuba triggered by the M w 8.8 Maule and M w 9.0 Tohoku-Oki earthquakes. *Bulletin of the Seismological Society of America*, *103*(1), 595-600.

[26] Peng, Z., Walter, J. I., Aster, R. C., Nyblade, A., Wiens, D. A., & Anandakrishnan, S. (2014). Antarctic icequakes triggered by the 2010 Maule earthquake in Chile. *Nature Geoscience*, *7*(9), 677.

[27] Peng, Z., Li, C., Walter, J., Ji, M., Liu, G., & Aster, R. (2019). Remote Triggering of Microseismicity at Mt. Erubus, Antarctica, Seismological Research Letters, 90(2B), 1042.

[28] Pollitz, F. F., Stein, R. S., Sevilgen, V., & Bürgmann, R. (2012). The 11 April 2012 east Indian Ocean earthquake triggered large aftershocks worldwide. *Nature*, *490*(7419), 250.

[29] Podolskiy, E. A., & Walter, F. (2016). Cryoseismology. *Reviews of geophysics*, *54*(4), 708-758.

[30] Walker, D. A., McCreery, C. S., & Hiyoshi, Y. (1992). T-phase spectra, seismic moments, and tsunamigenesis. *Bulletin of the Seismological Society of America*, *82*(3), 1275-1305.

[31] Wang, W., Meng, X., Peng, Z., Chen, Q. F., & Liu, N. (2015). Increasing background seismicity and dynamic triggering behaviors with nearby mining activities around Fangshan Pluton in Beijing, China. *Journal of Geophysical Research: Solid Earth*, *120*(8), 5624-5638.

[32] West, M., Sánchez, J. J., & McNutt, S. R. (2005). Periodically triggered seismicity at Mount Wrangell, Alaska, after the Sumatra earthquake. *Science*, *308*(5725), 1144-1146.

[33] Wu, J., Peng, Z., Wang, W., Gong, X., Chen, Q., & Wu, C. (2012). Comparisons of dynamic triggering near Beijing, China following recent large earthquakes in Sumatra. *Geophysical Research Letters*, *39*(21).